Fiber coupled sub nanometer displacement interferometry without periodic nonlinearity

Arjan J.H. Meskers[1], Jonathan D. Ellis[1,2], Jo W. Spronck[1,*], and Robert H. Munnig-Schmidt[1]

1 PME: Mechatronic System Design, Delft University of Technology, Mekelweg 2, 2628 CD Delft, The Netherlands
2 Now at: Mechanical Engineering Department & Institute of Optics, University of Rochester, Hopeman Building, Rochester, NY, 14627, USA
* Corresponding Author / E-mail: j.w.spronck@tudelft.nl, TEL: +31-15-278-1824, FAX: +31-15-278-2150

KEYWORDS : Displacement Interferometry, Fiber Coupling, Periodic Nonlinearity, Stage Metrology

Displacement interferometers are widely used in precision engineering and metrology applications. For multi-axis systems, free space delivery of the optical beams requires high tolerance pointing stability and couples the source to the interferometer location. Fiber delivery is desired to decouple the source and interferometer but configurations which have to be used for this, contribute typical errors such as periodic nonlinearity. In this paper, we describe a fiber-coupled Joo-type interferometer. Spatial separation of the input beams in this type of interferometer eliminate periodic nonlinearities. This is contrasted by typical heterodyne interferometer systems which have two orthogonal, coaxial beams with a difference frequency. We present the interferometer design, discuss the fiber deployment, and compare free-space and fiber-coupled versions. The results indicate that fiber-induced disturbances are rejected as theory predicts and no periodic nonlinearity was detected.

Manuscript received: January XX, 2011 / Accepted: January XX, 2011

1. Introduction and Motivation

Heterodyne displacement measuring interferometry has been widely used to calibrate other measurement tools such as capacitive sensors, inductive sensors, and optical encoders because of its high dynamic range, high signal-to-noise ratio, and direct traceability to the length standards [1]. Sub-nanometer level measurements must be achieved to satisfy industrial demands on performance [2]. The main error sources that limit the performance are the laser frequency stability [1], refractive index fluctuations in non-common optical paths [3], and periodic nonlinearity [4-6] in the measured phase due to source mixing, manufacturing tolerances, and imperfect alignment.

While the effects of the laser frequency stability and refractive index fluctuations can be mitigated by employing a highly stable reference laser and by performing the measurements in a well controlled environment, the periodic nonlinearity is difficult to eliminate. Moreover, for practical, modular interferometry systems, fiber delivery is desired to decouple the laser source (essentially a large heat source) from the interferometer. Decoupling the laser and interferometer also removes pointing stability effects between the two.

In this paper, we present a comparison between a free-space delivered and a polarization maintaining-fiber (PM-fiber) delivered generalized Joo-type interferometer, developed at the TU Delft. This interferometer type builds on previous research, as presented at the ISMTII in 2009 [7], which demonstrated no detectable periodic nonlinearity (down to the noise floor) in a practical interferometer configuration [8, 9]. The generalized Joo-type interferometer uses two spatially separated source beams with a known frequency difference, rather than the traditional coaxial, orthogonally polarized source beam. By eliminating all beam overlaps until the final interference element, periodic nonlinearity is significantly reduced [10-13]. However, when fiber delivery is applied, the extinction ratio of the fibers and stress induced birefringence can cause frequency mixing which will re-introduce the originally avoided periodic nonlinearity. Additionally, small fiber length changes will appear as Doppler shifts in the main interference signal and can be misinterpreted as stage motions. This interferometer configuration has several advantageous features which can be leveraged to reduce these effects. Simple polarization cleanup on the input beams can limit the fixing due to the fibers. Also, an optical reference is generated within the interferometer block, which will eliminate fiber-induced Doppler shifts and can reduce periodic nonlinearity [14, 15].

2. Modular Fiber Coupled System Concept

System modularity plays an important role for practical purposes in industry. Creating a modular 'plug-and-play' system will decrease system set up time and errors. Current free space systems lack this

robustness and are time consuming during installation due to high demands on pointing stability and alignment over long optical paths. The modular system proposed in this paper, as shown in Figure 1, utilizes fiber coupled delivery of source light towards the interferometer and fiber coupled delivery of the measurement signals to the phasemeter. Additionally, for these experiments, the initial heterodyne optical reference signal is generated at the source to assess fiber-induced Doppler shifts. This concept reduces the pointing stability requirements to just the tolerances in the optic block itself, rather than all components between it and the source. Also, fibers provide simple, flexible beam routing rather than fixed mirrors and splitters which require stable mounting and potentially unstable alignment mechanisms.

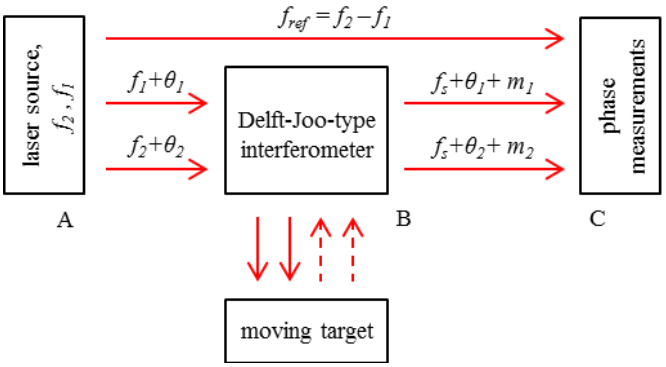

Figure 1: Schematic of the modular interferometry system using fiber couplings to eliminate high alignment accuracy, in between source (A), interferometer (B), and phasemeter (C).

The measurement system proposed can be divided up into three different modules to form the complete system. Module A contains the stabilized laser, components to generate two spatially separated input beams, f_1 and f_2 and the optical reference signal before the fibers, f_{ref}. The beams for the interferometer are then launched into PM-fibers while the optical reference is launched into multimode-fibers (MM fibers). The fiber-fed input beams are then sent to the interferometer, which is described in more detail in the next section. The interference signals, both from the interferometer and optical reference, are sent via MM-fibers to a phasemeter. The optical reference frequency is directly connected to the phasemeter (N1225A, Agilent) for phase measurement and post processing to determine the fiber-induced effects.

Figures 2 and 3 show the heterodyne frequency generation schematic and a photograph of our implementation, respectively. A frequency stabilized 633 nm HeNe laser is isolated from feedback using a free space optical isolator, OI. The beam is then split equally (BS_1) and each beam is frequency upshifted by an AOM, one at 39 MHz and the other at 41 MHz.

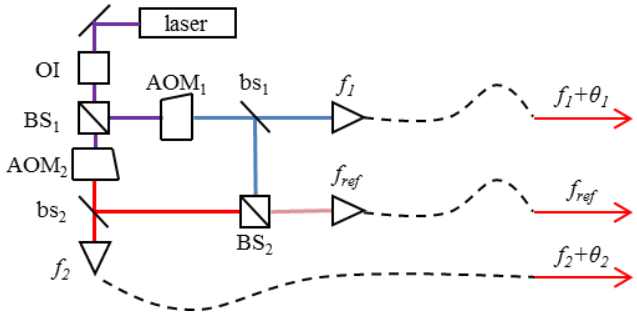

Figure 2: Schematic of the source and heterodyne frequency generation. A stabilized laser is optically isolated and split equally before passing through two AOMs driven at 39 MHz and 41 MHz, respectively. Both first order upshifted beams are transported to the interferometer, while also an optical reference signal is generated.

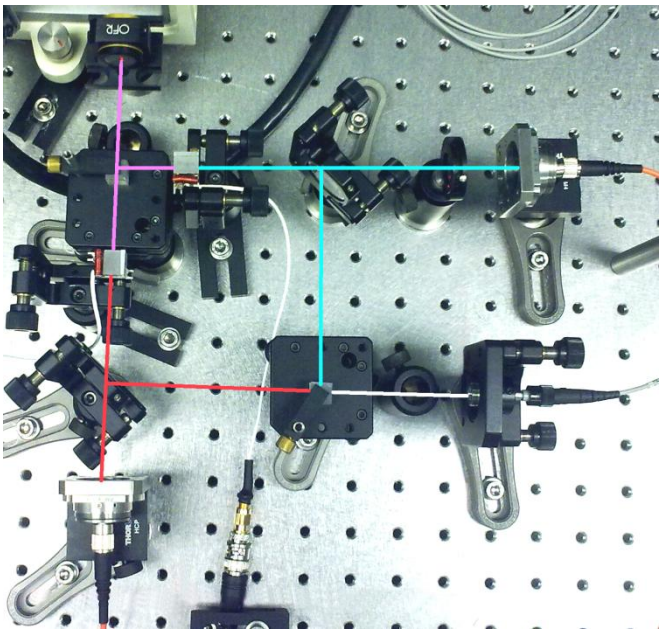

Figure 3: Photograph of our heterodyne frequency generation scheme.

An optical reference is generated at 2 MHz by using two beam samplers ($bs_{1,2}$) and a beamsplitter (BS_2) to interfere the upshifted beams. The main parts of each upshifted beam is either steered into the interferometer (in the free-space system) or launched into two PM fibers (for the fiber coupled system).

3. Generalized Joo-interferometer Design

Periodic nonlinearities are typically eliminated in heterodyne interferometry systems by only allowing the reference and measurement arms to overlap at the main interfering element [refs]. In all other instances, the beams remain separate. Figure 4 shows a schematic of the Generalized Joo-type interferometer used in this research. The two spatially separated input beams ($f_1+\theta_1$, $f_2+\theta_2$) with a slightly different optical frequency are sent to the interferometer. Two reference arms are generated by splitting 50% from a beam splitter (BS) and passing them to a large retroreflector (RR). The two beams reflect diagonally from the (large) RR and are shifted to a lower plane upon exiting, going into PD_m and PD_r and serve as reference beams. They then pass back to the BS where they interfere with their respective measurement arms.

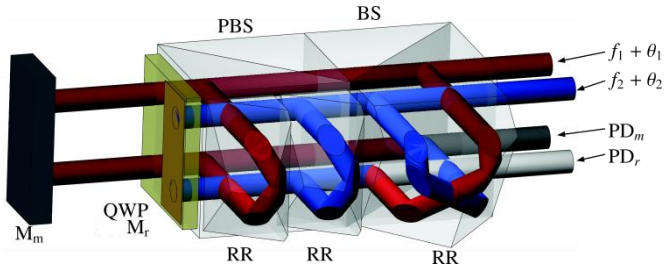

Figure 4: Schematic of the Generalized Joo-type interferometer. Two spatially separated input beams are sent to the interferometer which has a measurement interferometer and a reference interferometer to remove fiber-induced Doppler shifts. (In our implementation, a single right angle prism was used instead of two small retroreflectors for simplicity.)

The measurement arms are generated from the beams that initially transmit through the BS and transmit through a polarizing beam-splitter (PBS) and quarter wave plate (QWP) on the way to their respective mirrors. One is a fixed mirror to generate the reference

signal (M_r) and the other is a mirror mounted to the moving stage (M_m). Upon reflecting, both beams pass through the QWP for a second time where they reflect in the PBS. The beams reflect from two smaller RRs and are displaced to the same lower plane as their reference beams were displaced in the big RR. They then reflect in the PBS again and transmit through the QWP, where they hit their respective targets for a second time. They then transmit through the QWP, PBS and interfere with their reference arms in the BS. In our specific implementation, we replaced the two smaller RRs with a right angle prism (RAP), which performs essentially the same function.

Two signals, I_m and I_r are detected from fiber-coupled photo-detectors PD_m and PD_r, respectively. The two interference signals take the form of

$$I_m \propto \cos\left(2\pi f_1 t + \theta_1\right) \cdot \cos\left(2\pi f_2 t + \theta_2 + \theta_m\right) \quad (1)$$

$$I_r \propto \cos\left(2\pi f_2 t + \theta_2\right) \cdot \cos\left(2\pi f_1 t + \theta_1 + \theta_r\right) \quad (2)$$

where f_1 and f_2 are the two optical frequencies from the source, θ_1 and θ_2 are the phases of the two input beams (continuously changing due to the air-path/fibers, with $\theta_1 \neq \theta_2$), and θ_m and θ_r are the measured Doppler shifts due to mirror displacements. According to the trigonometric identity

$$2\cos A\cos B = \cos\left(A+B\right) + \cos\left(A-B\right) \quad (3)$$

Equations (1) and (2) can be rewritten with the additive components ignored because their frequencies are too high to detect. The resulting interference signals are

$$I_m \propto \cos\left(2\pi\left(f_1 - f_2\right)t + \theta_1 - \theta_2 - \theta_m\right) \quad (4)$$

$$I_r \propto \cos\left(2\pi\left(f_2 - f_1\right)t - \theta_1 + \theta_2 - \theta_r\right) \quad (5)$$

Assuming $f_1 - f_2 = f_s$, which is the 2 MHz split frequency, Equations (4) and (5) can be rewritten as

$$I_m \propto \cos\left(2\pi f_s t + \theta_1 - \theta_2 - \theta_m\right) \quad (6)$$

$$I_r \propto \cos\left(2\pi f_s t + \theta_1 - \theta_2 + \theta_r\right) \quad (7)$$

Using a similar procedure, it can be shown the irradiance of the optical reference signal, I_{or} , which is generated prior to the beam transport, is

$$I_{or} \propto \cos\left(2\pi f_s t\right) \quad (8)$$

If the optical reference is used for the phase measurement, then the difference between the phase fluctuations in the fibers appears as a Doppler shift in the measurement. However, the phase difference between I_m and I_r includes the fiber-induced phase changes, which cancels when the difference is measured ($(\theta_1-\theta_2+\theta_r)-(\theta_1-\theta_2-\theta_m) = (\theta_r+\theta_m)$). When the reference mirror is stationary ($\Delta\theta_r$ is zero), which is assumed for most displacement interferometers, the measured phase change equals the phase change of the measurement path ($\Delta\theta_m$). Assuming the refractive index and wavelength are constant, the measured phase change is then

$$\Delta\theta_m = \frac{2\pi N n \Delta x}{\lambda_2} \quad (9)$$

where N is the interferometer fold constant (four in this interferometer), n is the refractive index, λ_2 is the wavelength, and Δx is the displacement of the measurement mirror.

4. Free Space Generalized Joo-Interferometer System

The Generalized Joo-type interferometer was constructed using free space beam delivery and fiber-coupled detection, which can be seen in Figures 5 and 6. The measurement mirror was mounted to a linear air bearing stage (ABL1000, Aerotech), which has a 100 mm displacement range. Each measurement consists of a forward stage displacement, followed by a pause, and then a backwards stage displacement, all performed at constant velocity. During the stage displacement the mirror moved with a constant velocity, measurements were performed at 10 nm/s, 100nm/s, 1 µm /s, 10 µm /s and 100 µm/s.

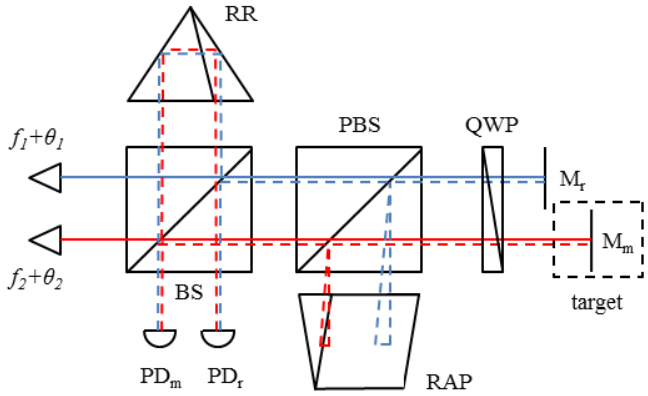

Figure 5: Schematic of the Generalized Joo-type interferometer. The spatially separated source beams come in including the phases θ_1 and θ_2 originating from either air-path or fiber induced disturbances. Detection takes place with PD_m and PD_r which are MM-fiber coupled to the phase meter (Agilent N1225A).

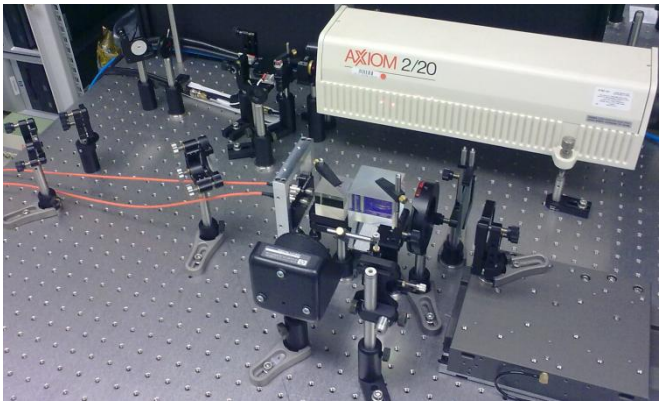

Figure 6: Photograph of the free space delivery system, interferometer and stage measurement setup. The two interference beams from the interferometer are detected and measured using MM-fiber and fiber-coupled detectors. The generation of the reference signal as depicted in Fig. 2 is not used in this setup.

The sampling rate and stage displacements are coupled in our case because only a limited number of points can be sampled using our interface with the phasemeter. At each velocity we sampled the maximum number of points (around 700k data points) and ensured that the sample rate was sufficient to measure and assess second order periodic nonlinearity in the measurements.

Figure 7 shows the displacement measured with the stage moving at a constant velocity of 10 nm/s. "Joo Gen" is the measured length change from the phase difference between I_r and I_m from PD_r and PD_m respectively. The Joo Gen signal closely follows the stage drive signal ("Path"), with minor fluctuations due to acoustic interference and refractive index changes. The relative error of these fluctuations decreases as the stage moves at higher velocity, as shown in Figure 8.

The linear forwards and backwards section were analyzed for each of the different velocities. Figure 9 shows the amplitude spectrum for the 100 μm/s velocity measurement as a function of Fringe Order which is typically used to analyze periodic errors.

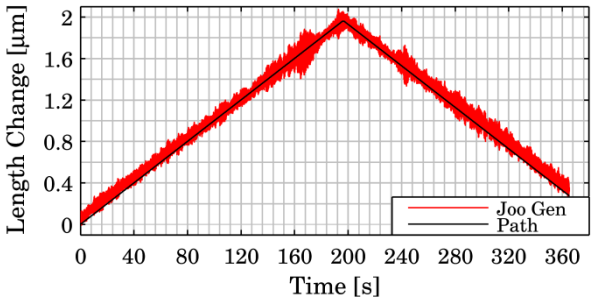

Figure 7: Stage measurement at 10 nm/s forwards and backwards. The air-path-induced Doppler shifts cause errors at nanometer level which clearly shows up at low velocities.

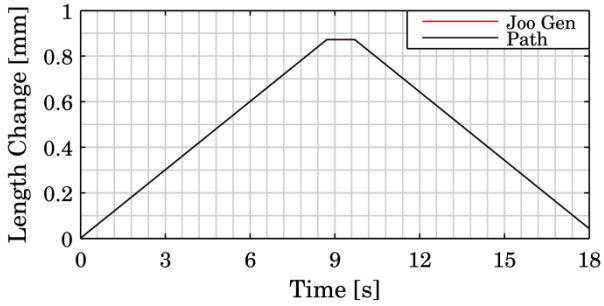

Figure 8: At 100 μm/s forwards and backwards, the air-path fluctuations are much smaller relative to the overall motion. The measured path and commanded path both nominally overlap.

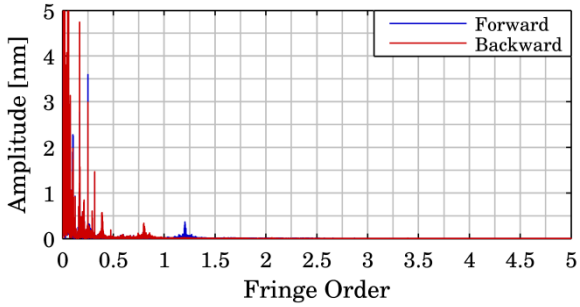

Figure 9: Periodic error analysis of the free-space 100 μm/s measurement. The amplitude spectrum after removing a first order polynomial and converting to the frequency domain for fringe spacing revealed no detectable periodic errors.

In this measurement, there are clearly no first or second order periodic errors present and the peaks at the lower fringe orders are due to noise in the surrounding environment. This measurement is indicative of the other measurements taken spanning from 10 nm/s to 1 mm/s. In all measurements, the only peaks that occurred at the first and second fringe orders occurred due to vibrations coincidentally overlapping because the fringe passing frequency and vibration frequencies were matched.

The noise in the surrounding environment that was observed in all measurements lays around 34 Hz, see Figure 14. This noise is attributed to laboratory acoustic interference, vibrations, and refractive index fluctuations, which also have been observed in other measurements in the laboratory.

5. Fiber Coupled Generalized Joo-Interferometer System

The Generalized Joo-type interferometer as shown in Figure 5 was tested at the same velocities as its free-space counterpart. Figure 10 shows a photograph of the fiber-coupled setup. The phase differences between I_r, I_m, and I_{ref} were all measured to assess both the fiber fluctuations and the stability of the reference arm in the interferometer.

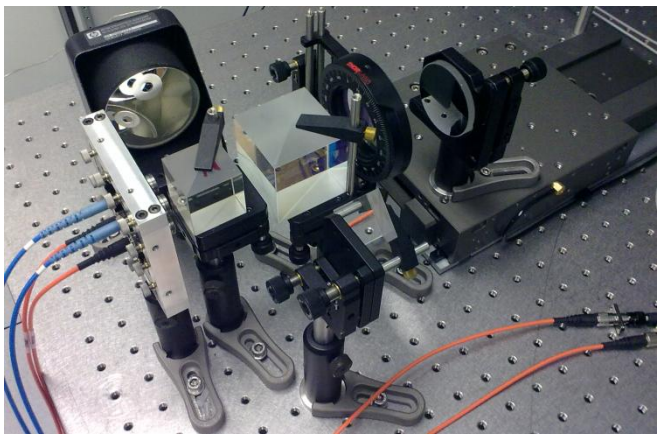

Figure 10: Photograph of our measurement setup with PM fiber coupled source beam delivery. The setup and detection are identical to the scheme in Fig. 4 and the setup in Fig. 5 except for the fiber delivery.

Figure 11 shows the measured displacement with the stage moving at a constant velocity of 10 nm/s. Displacement "Ref" is the measured length change from the phase difference between difference between I_{ref} and I_r. "Meas" is the difference between I_{ref} and I_m. Both of these signals show considerable drift which is can be attributed to fiber-induced Doppler shifts. "Joo Gen" is the measured length change from the phase difference between I_r and I_m, which cancels the fiber-induced Doppler shifts. The Joo Gen signal follows the stage drive signal ("Path"), with small fluctuations due to acoustic interference and refractive index fluctuations. When the fiber effects are not canceled and the stage motion is slow, the fibers can induce large errors. When the stage velocity is higher, as shown in Figure 12 where the velocity is 100 μm/s, the fiber fluctuations are smaller, but still cause errors on the micrometer level if it is not taken into account.

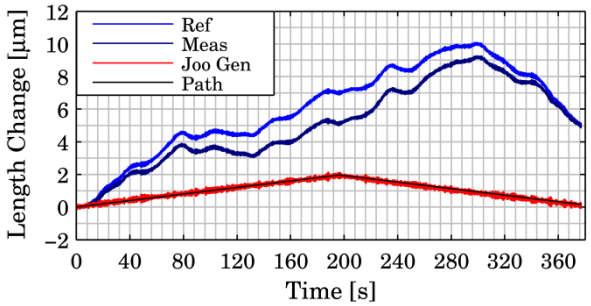

Figure 11: Stage measurement at 10 nm/s forwards and backwards. The fiber-induced Doppler shifts cause errors at the micrometer level which can be clearly seen at low velocities.

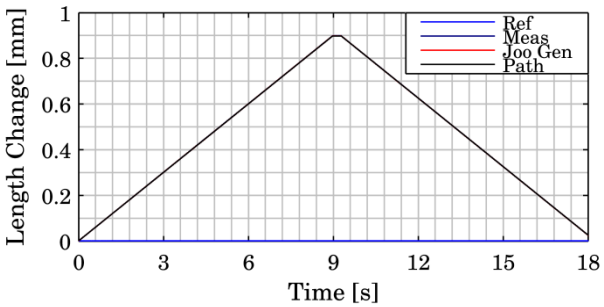

Figure 12: At 100 μm/s forwards and backwards, the fiber fluctuations appear much smaller relative to the overall motion but still contribute errors on the order of micrometers. Meas, Joo Gen, and Path all nominally overlap in this instance.

Also for this interferometer configuration, the linear forwards and backwards section were analyzed for each of the different velocities. Figure 15 shows the amplitude spectrum as a function of Fringe Order for the 100 µm/s velocity measurement which clearly shows no observable periodic errors.

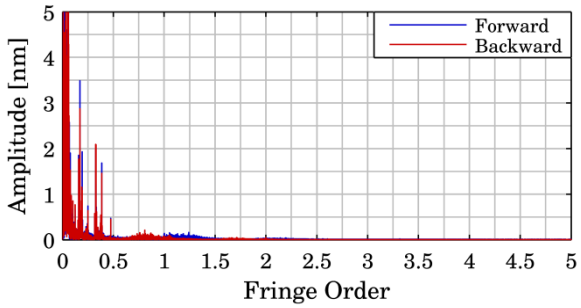

Figure 13: Periodic error analysis of the fiber-coupled 100 µm/s measurement. Correlation with the frequency domain for fringe spacing revealed no detectable periodic errors.

When the frequency spectrum is converted to Fringe Order based on the nominal fringe spacing, also for this measurement setup, the peaks shift with an order of magnitude spacing between them, as shown in Figure 15. From the results from the fiber coupled measurements peaks can be observed at the first and second order harmonics, which shift when different sampling and velocity parameters are changed. This means the peaks also here are not attributed to periodic nonlinearity. Thus, we conclude that this interferometer configuration in both its free-space and fiber-delivered configuration has no detectable periodic nonlinearity.

Figure 16 shows a comparison between free-space and fiber coupled measurements at 100 µm/s. The free-space measurement shows sharper peaks in the amplitude spectrum than the fiber-coupled version. Because the fibers create a continuous frequency shift at the micrometer level, some peaks are attenuated which can be advantageous for high frequency feedback stages. The lower order vibrations are likely due to the surrounding environment while the symmetric peaks around the first order are due to stage motions. The forwards and backwards motions of the stage cause opposite Doppler shifts, which will be reflected in the measurement if the stage motion or mirror mount on the stage are vibrating due to the motion.

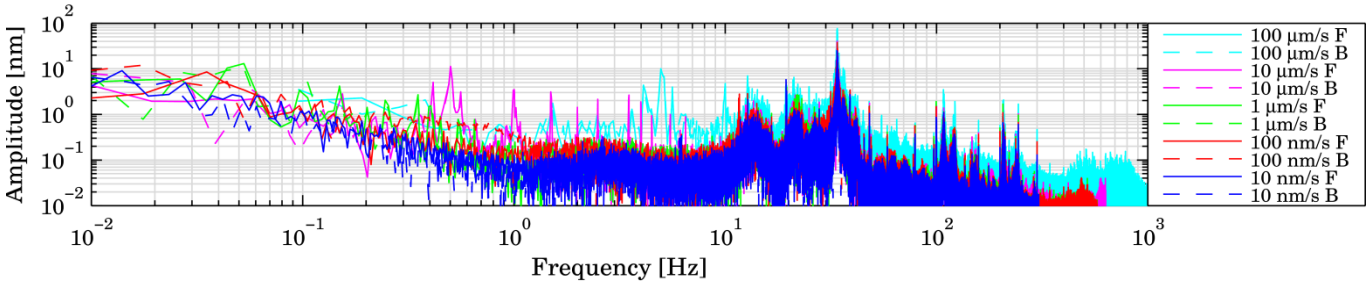

Figure 14: Amplitude spectrum based on the sampling frequency for various stage motion velocities. There is a common noise level in the range of 10 Hz to 40 Hz and at higher peaks which can be seen in all measurements. The higher noise levels in the faster measurements (100 µm/s and 10 µm/s) is likely due to increased vibrations from the stage motion and instability in the mirror mount.

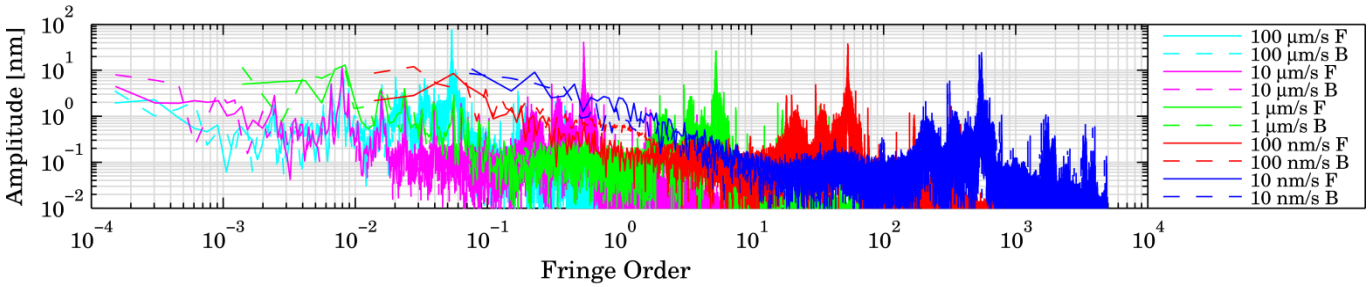

Figure 15: Amplitude spectrum based on the fringe passing frequency to determine the error amplitude based on Fringe Order. Typically periodic nonlinearity occurs at the first and second fringe orders. Because these peaks shift as a function of velocity but not sampling frequency, they can be attributed to vibrations rather than periodic error. This is particularly for the 1 µm/s measurements which has a clear peak at the first fringe order but has matched peaks shifted by an order of magnitude as the velocity changes by equal order of magnitude.

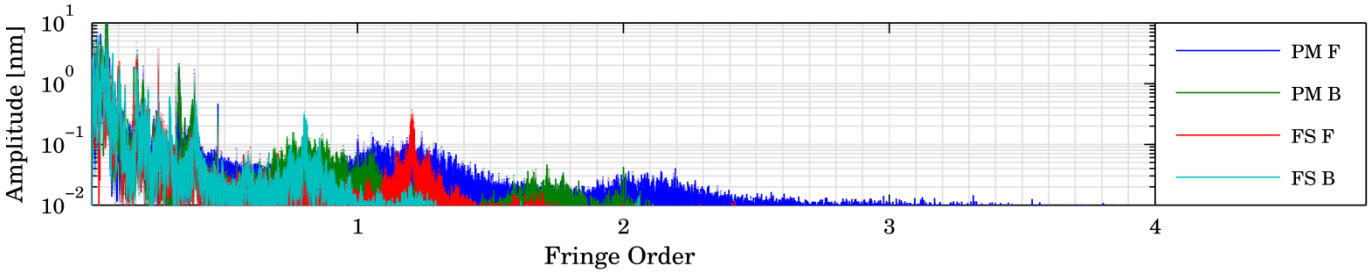

Figure 16: Amplitude spectrum of Figures 9 and 13 combined. The peaks for the free-space setup are much sharper than the broad ‘peaks’ from the fiber coupled setup. The forward and backward travel of the stage shows symmetry around a fringe order of 1 which is related to the positive and negative Doppler shift depending on the direction of stage travel.

6. Conclusions

Two types of beam delivery were designed, built, and tested for the Generalized Joo-type interferometer, one with free-space delivery and one with PM optical fiber delivery. The free-space and fiber-delivered systems used essentially the same components, with the exception of the fiber couplers themselves and beam steering mirrors for the free space setup. The fiber coupled system has an advantage of being completely decoupled from the source, while still contributing no periodic nonlinearity and self correcting for false fiber-induced displacements.

Measurements with the fiber coupled configuration have showed that the system is capable of operating at the same or at a lower noise level than the free-space beam delivery setup. Linear displacements and frequency domain analysis techniques were employed to assess the periodic nonlinearity and deconvolve it from spurious vibrations and refractive index fluctuations.

This research shows a highly modularized displacement interferometry system without free-space beam delivery paths, which can be suitable for sub-nanometer measurements.

ACKNOWLEDGEMENTS

This work was performed at the Delft University of Technology and supported by the Dutch IOP (IPT04001) in the Netherlands. The authors are grateful for the support by Agilent Technologies for providing the phase measurement board used during these measurements. The authors would like to thank the IOP User Committee for many fruitful discussions regarding this research.

REFERENCES

1. Bobroff, N., “Recent advances in displacement measuring interferometry”, Measurement Science and Technology, Vol. 4, No. 9, pp. 907-926, 1993.
2. Demarest, F.C., “High-resolution, high-speed, low data age uncertainty, heterodyne displacement measuring interferometer electronics”, Measurement Science and Technology, Vol. 9, No. 7, pp. 1024-1030, 1998.
3. Tyler Estler, W., “High-accuracy displacement interferometry in air”, Applied Optics, Vol. 24, No. 6, pp. 808-815, 1985.
4. Quenelle, R.C., “Nonlinearity in interferometer measurements”, Hewlett Packard Journal, Vol. 34, pp 10, 1983.
5. Hou, Wenmei, Wilkening and Gunter, “Investigation and compensation of the nonlinearity of heterodyne interferometers”, Precision Engineering, Vol. 14, No. 2, pp 91-98, 1992.
6. De Freitas, J. M. and Player, M. A., “Polarization Effects in Heterodyne Interferometry”, Journal of Modern Optics,Vol. 42, No. 9, pp. 1875-1899, 1995.
7. Joo, K.N., Ellis, J.D., Spronck, J.W., van Kan, P.J.M. and Munnig Schmidt, R.H., “Simple heterodyne laser interferometer without periodic errors”, Proc. 9th ISMTII, 29 Jun-2July, St. Petersburg, Russia, 2009.
8. Joo, K.N., Ellis, J.D., Spronck, J.W., van Kan, P.J.M. and Munnig Schmidt, R.H., “Simple heterodyne laser interferometer with subnanometer periodic errors”, Optics Letters, Vol. 34, No. 3, pp. 386-388, 2009.
9. Joo, K.N., Ellis, J.D., Spronck, J.W., Buice, E.S., Spronck, J.W. and Munnig Schmidt, R.H., “High resolution heterodyne interferometer without detectable periodic nonlinearity”, Optics Express, Vol. 18, No. 2, pp. 1159-1165, 2010.
10. Tanaka, M., Yamagami, T. and Nakayama, K., “Linear interpolation of periodic error in a heterodyne laser interferometer at subnanometer levels [dimension measurement]”, IEEE Transactions on Instrumentation and Measurement, Vol. 38, No. 2, pp. 552-554, 1989.
11. Wu, C., Lawall, J., and Deslattes, R.D., “Heterodyne Interferometer with Subatomic Periodic Nonlinearity”, Applied Optics, Vol. 38, No. 19, pp. 4089-4094, 1999.
12. Lawall, J., and Kessler, E., “Michelson interferometry with 10 pm accuracy”, Review of Scientific Instruments, Vol. 71, No. 7, pp. 2669-2676, 2000
13. Schuldt, H., Gohlke, M., Weise, D., Johann, U., Peters, A. and Braxmaier, C., “Picometer and nanoradian optical heterodyne interferometry for translation and tilt metrology of the {LISA} gravitational reference sensor”, Classical and Quantum Gravity, Vol. 26, No. 8, pp. 085008, 2009.
14. Knarren, B.A.W.H., “Application of optical fibres in precision heterodyne laser interferometry”, PhD Thesis, Technical University of Eindhoven, Netherlands, 2003.
15. Knarren, B.A.W.H., Cosijns, S.J.A.G., Haitjema, H., and Schellekens, P.H.J., “Validation of a single fibre-fed heterodyne laser interferometer with nanometre uncertainty”, Precision Engineering, Vol. 2, pp. 229-236, 2005